Available online at website: https://journal.bcrec.id/index.php/bcrec

Bulletin of Chemical Reaction Engineering & Catalysis, 20 (1) 2025, 143-155

Research Article

Enhancing Carbon Monoxide Oxidation of Cobalt-Nickel Containing A-Deficient Perovskites through Exsolution Agents and Reduction-Oxidation Pretreatment

Lew Guo Liang[1], Wan Khairunnisa Wan Ramli[1,3*], Naimah Ibrahim[2,3], Sureena Abdullah[4]

[1]Faculty of Chemical Engineering & Technology, Universiti Malaysia Perlis, Kompleks Pusat Pengajian Jejawi 3, 02600 Arau, Perlis, Malaysia
[2]Faculty of Civil Engineering & Technology, Universiti Malaysia Perlis, Kompleks Pusat Pengajian Jejawi 3, 02600 Arau, Perlis, Malaysia
[3]Centre of Excellence for Water Research and Environmental Sustainability Growth (WAREG), Universiti Malaysia Perlis, Arau, Perlis, Malaysia
[4]Faculty of Chemical and Process Engineering Technology, Universiti Malaysia Pahang Al-Sultan Abdullah, Lebuhraya Persiaran Tun Khalil Yaakob, 26300 Kuantan, Pahang Darul Makmur, Malaysia

Received: 6th December 2024; Revised: 15th February 2025; Accepted: 15th February 2025
Available online: 19th February 2025; Published regularly: April 2025

Abstract

In this work, different types of exsolution agents and pretreatment processes, comprising reduction-oxidation (RO) components, were introduced to modulate the exsolution process of A-deficient perovskites, $La_{0.7}Ce_{0.1}Co_{0.3}Ni_{0.1}Ti_{0.6}O_3$. The catalysts were assessed using field emission scanning electron microscopy with energy dispersive spectroscopy (FESEM/EDS), X-ray Diffraction (XRD) and X-ray photoelectron spectroscopy (XPS). Their carbon monoxide (CO) oxidation activity was also compared. The results showed that the catalytic activity degraded at 520 °C when hydrogen (E-H) was used as the exsolution agent. When RO components were introduced as exsolution agents (E-CO/O_2) or in the pretreatment (RO2% and RO18%), the deactivation at high temperatures was mitigated. The results of this study showed that RO18% was favourably pretreated with RO components, recording the highest CO conversion of 60.57% at 520 °C and across all temperatures with no degradation at high temperature. It also recorded the lowest activation energy of 14.449 kJ/mol. The EDS, XRD, and XPS analyses of the catalyst demonstrated that the active sites for this reaction are primarily Co^{2+} with Ni serving as the anchor between the metals and perovskites support. A high amount of lattice oxygen (O_2) with higher binding energy and chemisorbed O_2 species also influenced the improved catalytic activity, attracting CO for reaction, reacting with the available surface O_2 and the faster replenishment of O_2 vacancies by the absorbed and bulk O_2 lattice. These findings highlight the prospects of CO and O_2 inclusion in pretreatment for perovskite catalyst as options to reduce metal agglomeration and further improve CO oxidation activity.

Keywords: Pretreatment; Exsolution; Transition metals; CO oxidation; Surface oxygen

How to Cite: Liang, L. G., Ramli, W. K. W., Ibrahim, N., Abdullah, S. (2025). Enhancing Carbon Monoxide Oxidation of Cobalt-Nickel Containing A-Deficient Perovskites through Exsolution Agents and Reduction-Oxidation Pretreatment. *Bulletin of Chemical Reaction Engineering & Catalysis*, 20 (1), 143-155. (doi: 10.9767/bcrec.20262)

Permalink/DOI: https://doi.org/10.9767/bcrec.20262

1. Introduction

Transition metals assume a crucial role in catalysis, functioning as indispensable constituents in numerous chemical reactions owing to their distinctive electronic configurations and capacity to facilitate electron transfer [1]. Their catalytic performance is commonly ascribed to their ability to transition between different oxidation states, create coordination complexes, and involve themselves in diverse bonding interactions [2]. Nevertheless, the application of

* Corresponding Author.
Email: wankhairunnisa@unimap.edu.my (W.K.W. Ramli)

transition metals in catalytic mechanisms is accompanied by certain obstacles. One notable limitation is the tendency of these metals to agglomerate, especially when reaching high temperature, where individual metal particles merge, causing a diminished in active surface area and therefore result to a drop in catalytic effectiveness [3]. This decline not only reduced the catalyst's efficiency, but also affected the broader sustainability and economic feasibility of catalytic processes. It is imperative to comprehend the equilibrium between the beneficial characteristics of transition metals and the adverse effects coming from agglomeration to optimize their application in industrial contexts.

Perovskite oxides have a unique structure that is known to be capable of self-regenerating with good electronic properties that attract a significant amount of attention from researchers and industries as potential catalysts for diverse chemical reactions [4]. By itself, the ABO_3 structure is able to incorporate two transition metals as an oxide. In further development, a particularly intriguing formulation of perovskite oxides, A site-deficient perovskites, exhibited outstanding catalytic performances, particularly in carbon monoxide oxidation. The extraordinary catalytic performance of A-deficient perovskites can be ascribed to their capacity to accommodate a wide range of structural alterations, such as the manipulation of lattice vacancies and the stabilization of transition metals in different oxidation states within the structure [5,6]. The incorporation of A-site deficiencies within perovskite catalysts has been proven to augment their oxygen storage capacity and mobility, which are crucial elements that contribute to their improved catalytic efficiency. This enhanced the transportation of oxygen during reaction, improving oxygen vacancies and ensuring improved catalytic performance. Moreover, the capacity of A-deficient perovskites to stabilize different oxidation states of metal cations may also significantly influence their catalytic effectiveness, offering additional mechanisms for the generation of reactive oxygen species and the surface adsorption or activation of binding reactants [7].

One major setback in using these types of perovskite catalysts in catalysis is mainly due to the higher tendency of the active sites, commonly transition metals, to agglomerate, especially at higher temperatures. Although these types of perovskite catalysts can undergo post-reduction to restore the active sites, the stability of these sites remains a critical concern. Researchers have explored various strategies, including optimizing the synthesis conditions and employing different metal precursors, to enhance metal dispersion and prevent agglomeration during catalytic processes. Dai *et al.* [8] reported an improved reducibility of the $LaCoO_3$ catalyst, subsequently improving their CO oxidation activity by employing an acid etching method to tune the surface of the perovskite catalyst. Pinto and Glisenti [9] discovered that by doping $LaCoO_3$ with Strontium, Sr, a higher CO oxidation activity was measured than that of $LaCoO_3$, attributing to the improved reducibility of $LaCoO_3$-based perovskite oxides, resulting in lower activation energies for CO oxidation [10]. Redox pretreatments have also been extensively used to tune the structure of heterogenous catalysts, not limited to perovskites catalysts, for enhanced catalytic activity. Still, these pretreatments can also induce unpredictable structural changes that can lead to reduced catalytic activity. In other words, the selection of appropriate pretreatment methods is considered crucial in tuning perovskites catalysts as a way to understand their evolution towards enhancing catalytic activity. Jiang *et al.* [11] reported that by introducing oxidizing pretreatment, sufficient metallic Au and efficient metal-support interfacial sites were provided, contributing towards the enhanced CO oxidation activity and stability simultaneously.

In this work, the effects of various exsolution agent and redox pretreatment on the CO oxidation activity of the exsolved A-deficient CoNi perovskites catalysts were evaluated. The relationships between surface morphology, crystal structure, electronic configuration and catalytic activity were also established.

2. Materials and Methods

2.1 Materials

Metal nanoparticle precursors, such as Cobalt(III) oxide (Co_3O_4, 99.5%) and Nickel(II) nitrate hexahydrate ($Ni(NO_3)_2*6H_2O$, 99%), were purchased from Sigma Aldrich and Acros Organics, respectively. The precursors for the perovskites support, such as Lanthanum oxide (La_2O_3, 99.98%), Ceria oxide (CeO_2, 99%) and Titanium oxide (TiO_2, 99.9%) were also procured from Acros Organics, US. The gases, including 30% hydrogen/argon (H_2/Ar), 20% carbon monoxide/nitrogen (CO/N_2), 20% oxygen/nitrogen (O_2/N_2), and 99.999% nitrogen (N_2) were purchased from the Linde group. All chemicals and gases for experimental works were used as received.

2.2 Catalyst Preparation

The exsolved A-deficient CoNi perovskites catalysts with chemical compositions of $La_{0.7}Ce_{0.1}Co_{0.3}Ni_{0.1}Ti_{0.6}O_3$ were prepared via the common solid-state reaction previously described by Naegu *et al.* [12] with some modifications. Stoichiometric amounts of the high-purity precursors were mixed with acetone and heated in an oven at 200 ℃ to

remove any moisture and volatile substance before undergoing the calcination processes. The powders were then calcined in a furnace at 1000 °C for 12 hours in air to produce a pure perovskite structure. The exsolution of CoNi nanoparticles under three different exsolution conditions (Table 1); namely hydrogen gas (H_2), carbon monoxide (CO), and a mixture of carbon monoxide and oxygen (CO-O_2), was carried out in situ in a conventional continuous flow reactor (Figure 1), as described in our previous work [13]. This setup will also be used for RO pretreatment and catalytic activity measurement. A temperature of 550 °C and a duration of 5 hours were chosen to prevent any agglomeration caused by the over exsolution at higher temperatures (>550 °C), as reported in our previous works [13,14]. The exsolution agents were chosen based on previous study reported by Naegu et al, in which enhanced CO oxidation activity was observed when this type of catalysts is exposed in CO-O_2 environment [12].

An amount of 60 mg of the calcined powder was mixed with Al_2O_3 powder before progressing to exsolution and catalytic reaction. Inert alumina was used to ensure a reasonable pressure drop and uniform temperature distribution within the catalyst's bed and reactor. This also suppressed the dispersion of the powder during the reaction while acting as the filler for the catalysts. The reactor was placed horizontally in a temperature-controlled open furnace with a fixed heating rate of the bed of 5 °C/ min. The metal exsolution of the catalyst was performed by introducing the exsolution agent at a total flow rate of 250 mL/min

Table 1. Perovskites-supported CoNi catalysts with different exsolution agents and Reduction-Oxidation (RO) pretreatment conditions.

Catalyst	Exsolution agent	RO agent	Temperature (°C)	Duration (hours)
E-H	H_2-He	-	550	5
E-CO	CO-N_2	-	550	5
E-CO/O_2	CO-O_2	-	550	5
RO2%	H_2-He	2% CO-O_2	550	5
RO18%	H_2-He	18% CO-O_2	550	5

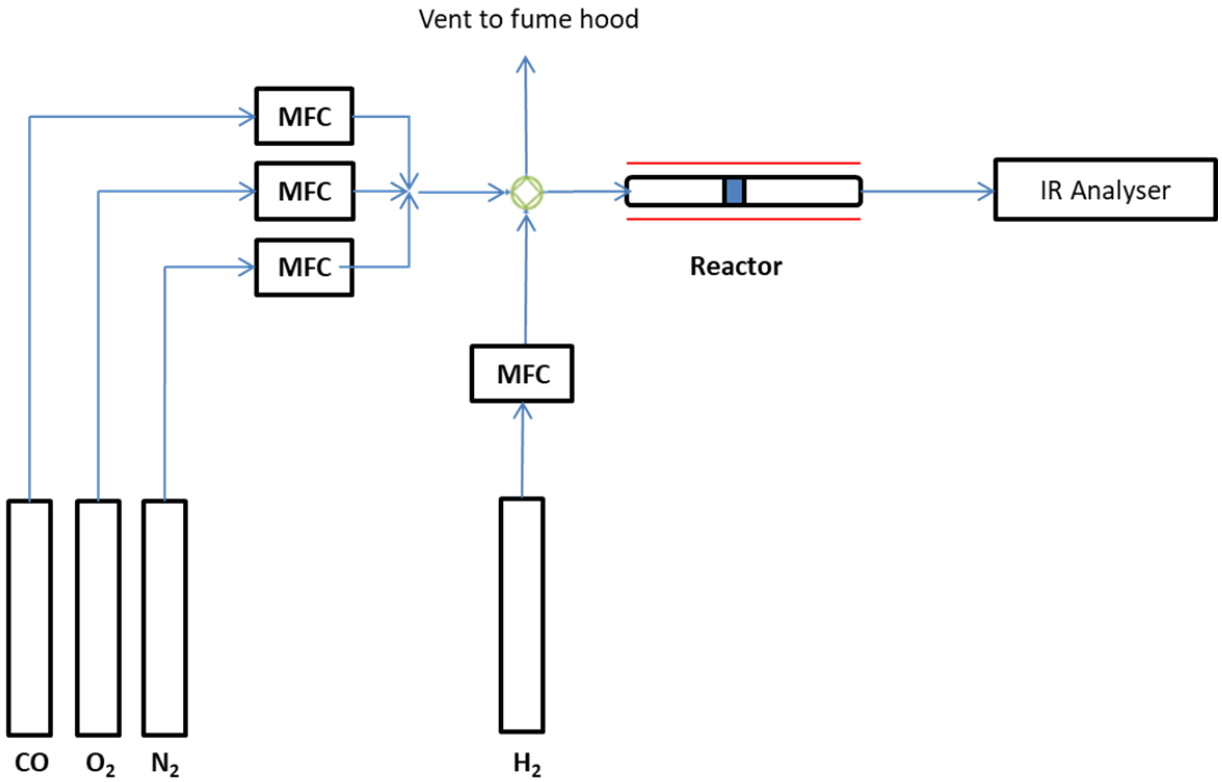

Figure 1. Reactor setup.

over the catalysts at 550 °C for 5 hours. For CO/O_2, a chemically reactive CO/O_2 mixture (18% CO, 1% O_2) at a total flow rate of 50 mL/min was introduced over the hot powders at the same temperature and duration. Digital gas flow meters were used to measure the flow rates of CO and O_2 feeds at the required amount. The catalyst was cooled to room temperature in the same exsolution atmosphere before proceeding into catalyst characterizations and catalytic activity measurement.

Pretreatment conditions were also evaluated, in particular, under reduction-oxidation (RO) environments as prior researches observed augmented catalytic activity of this type of catalyst upon exposure under RO conditions, attributing to the structural changes of nanoparticles, which are found to be more active towards CO oxidation. The RO pretreatment conditions of the prepared catalysts are listed in Table 1. After the CoNi exsolution with H_2 (E-H), the catalysts were exposed to two different RO conditions in the same reactor setup as the exsolution step at 550 °C for 5 hours; one with 2% CO and 1% O_2, and another with 18% CO and 1% O_2. These chemically active mixtures were introduced at a total flow rate of 250 mL/min when the temperature reached 550 °C and the flow rates were observed throughout the pretreatment process. The catalyst was cooled to room temperature in the same pretreatment condition before proceeding into catalyst characterizations and catalytic activity measurement.

2.3 Catalyst Characterizations

The surface morphology of the fabricated catalysts was evaluated using the Field emission scanning electron microscopy (FESEM) on a ZEISS SUPRA 55VP instrument operating at 3 kV. The chemical composition of the catalysts was also examined using the energy dispersive spectroscopy (EDS) attached to the FESEM. The X-ray diffraction (XRD) peaks were attained using Bruker D2 Phaser benchtop X-ray diffractometer (XRD), equipped with LYNEYE 1D Ultra-fast-solid-state detector with Cu-Kα radiation of 1.5418 Å between the $10°<2\theta<80°$ scanning range. The X-ray photoelectron spectroscopy (XPS) analysis of the catalysts was performed on a ULVAC-PHI 5000 VersaProbe II with monochromatic Al-K radiation of 1486.6 eV, while operating at the bean voltage of 15 kW. The binding energy was calibrated using a C 1s peak at 284.8 eV with an accuracy of ±0.1 eV as standard.

2.4 Catalytic Activity Evaluation

The catalytic activity evaluation of the catalysts under CO oxidation was performed using the same reactor setup as those used in the exsolution and pretreatment steps. 60 mg of catalyst, diluted with Al_2O_3 powder was exposed under the following reaction conditions: a feed gas mixture containing 2% CO and 1% O_2 gases, with a total flow rate, F_t of 250 $mL.min^{-1}$ given at normal temperatures. The evaluation of the catalytic activity of the catalysts as a function of temperature, also known as the light-off test was conducted to determine the effectiveness of the catalyst for CO oxidation. The reaction temperatures, ranging from room temperature to 520 °C, with a step size of 20 °C were used. Data was recorded after stable CO_2 production values were observed. The catalytic experiments were carried out under steady-state conditions and the flow rates of CO and O_2 were monitored with digital gas flow meters. The outlet stream was connected to an Infra-Red (IR) analyzer, equipped with CO, O_2, and CO_2 detectors and it was used to analyze the CO_2 production in ppm. The stoichiometric CO oxidation reaction can be represented by Equation (1):

$$CO + \frac{1}{2} O_2 \rightarrow CO_2 \quad (1)$$

The catalytic activity was expressed in terms of CO conversion and reaction rates. The CO conversion and reaction rates, $r^*_{CO_2}$, in terms of CO_2 production for all catalysts were calculated based on the following Equations (2) and (3), respectively:

$$\text{CO conversion}, \% = \frac{\text{CO}_2 \text{ produced (ppm)}}{\text{Total CO supply (ppm)}} \; x \; 100\% \quad (2)$$

$$r^*_{CO_2}(\mu mol\ (CO_2) s^{-1} g^{-1}) = \frac{y_{CO_2} \times \dot{n}}{w_p} \quad (3)$$

where, y_{CO_2} is the CO_2 concentration (ppm) measured by the IR analyzer at the gas outlet, $\dot{n}$ is the total molar flow rate of the reaction and w_p is the weight of the active catalysts (w_p = 60 mg).

The apparent activation energy of the catalyst was measured using the same reactor setup. According to the Arrhenius equation (Equation (4)):

$$\ln k = -\frac{E_a}{RT} + \ln A \quad (4)$$

where, k is the kinetic constant, E_a is the apparent activation energy, T is the reaction temperature, and A is a pre-exponential factor.

3. Results and Discussion

3.1. Catalysts Characteristics

The surface morphologies and the elemental analysis of the exsolved CoNi perovskites catalysts, prepared using three different exsolution agents are illustrated in Figure 2 (a-c).

E-H and E-CO exhibited a rather similar nano/ micro rectangular morphology with the latter illustrated a well-defined rectangular shape distributed across the image as compared to a mixed of rectangular/irregular shape demonstrated in E-H. In contrast, polyhedral-like nano/ microstructures were observed in E-CO/O_2, denoting that the O_2 presence weakened the exsolution power of CO. The exsolution process is slower compared to H_2, thus a mixture of polyhedral cluster and rectangular shapes were present as the polyhedral begins to emerge and eventually formed rectangular-shaped particles [15]. Similar nano/micro rectangular morphologies as those in E-H were observed in RO2% and RO18%, confirming the completion of the exsolution process.

The EDX analysis of the metal species, namely Co and Ni, is also presented in Figure 2 (f). A distinct comparison between the catalysts prepared with different exsolution agents can be made in terms of the amounts of exsolved Co and Ni, exhibiting their major effect on the amount of metal exsolved and on the microstructure of the catalysts [16]. H_2, as the stronger exsolution agent (E-H) advocates the exsolution of more Co metals, approximately four times the amount of Ni exsolved onto the perovskite surface, but when CO, a weaker exsolution agent was used as the exsolution agent, relatively similar exsolution rates were observed between Co and Ni, signifying the stronger effect of CO in exsolving Ni. When a small amount of O_2 was introduced (E-CO/O_2) as the exsolution agent along with CO, the exsolution rates for both Co and Ni increased, almost doubling the amount of Co exsolved when only CO was used. Comparable effects on the metal exsolution were observed with those of E-CO/O_2

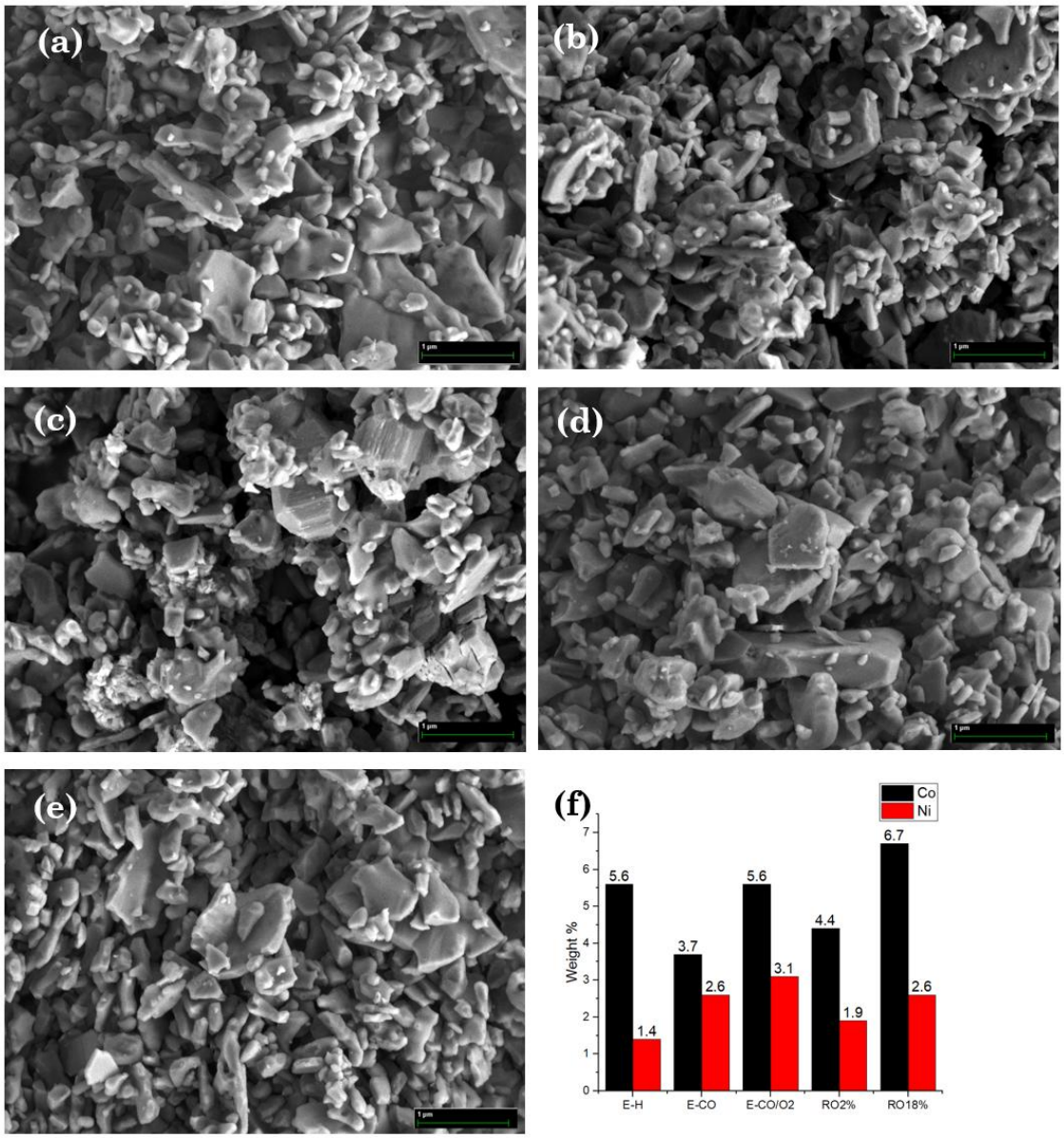

Figure 2. FESEM images of the perovskites-supported CoNi catalysts with different exsolution agents under 20k magnification with their respective EDX results: (a) E-H, (b) E-CO, (c) E-CO/O_2, (d) RO2%, (e) RO18%, and (f) elemental mapping of the catalysts.

when introducing the redox pretreatment on E-H catalysts (RO2% and RO18%). As the CO concentration was increased from 2 to 18%, the enhanced amount of Ni exsolved was also expected, proving yet again the strong effect of CO in exsolving Ni. The weight percentage of Ni increases from 1.4 to 1.9 and 2.6, resulting the Co/Ni ratio to be 2.32 and 2.57 for RO2% and RO18%, respectively.

Figure 3 illustrates the diffraction peaks of all catalysts to evaluate their corresponding crystal structure. All catalysts showed similar peaks at 2θ values close to 33˚, 41˚, 47˚, 59˚, and 69˚ that can be indexed to a rhombohedral hexagonal $LaCoO_3$, and this belongs to the space group R-3c ($LaCoO_3$, PDF code: 96-153-3634) [17]. These peaks indicate a successful incorporation of metals, especially Co into the perovskite lattice. Since the prepared catalysts were in the form of A-site-deficient perovskites, the changes in perovskite lattice were noticeable. The strongest diffraction peak for perovskite oxides which was located at 33˚ was shifted to a lower diffraction angle, possibly influenced by the addition of nickel causing the lattice to expand due to the larger ionic radius of Ni ions in comparison to those of Co ions [18].

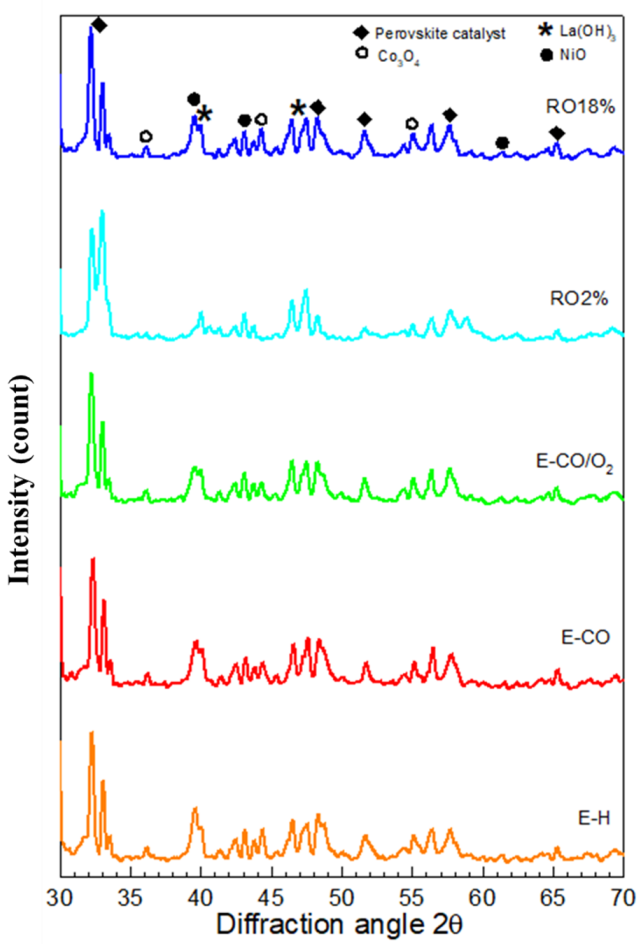

Figure 3. X-ray diffraction patterns for all perovskite catalysts with different exsolution agents and Reduction-Oxidation pretreatment.

Some traces of active metals were also detected, possibly dispersed on all catalysts. A trace of Co_3O_4 was detected at 37° and 44° [19] and several peaks that belong to NiO at 39°, 43°, and 62° [20] were also detected. Diffraction peaks attributed to $La(OH)_3$ impurities can also be detected at diffraction angles of 40° and 46° in all catalysts, resulting from a potential reaction between La_2O_3 and atmospheric moisture after calcination [21]. At 2θ region between 47°-48°, it was observed that the peaks' intensity increases with catalysts that were exposed to CO (E-CO, E-CO/O_2) or RO pretreatment (RO2% and RO18%), signifying that their crystallinity was positively influenced by higher cobalt presence in the perovskite lattice [17]. These results aligned with the EDX results, indicating an increase in cobalt content when the catalysts were exposed to CO or RO pretreatment during the exsolution process.

Figure 4 shows the XPS spectra for Co2p, Ni2p, and O1s for all five catalysts. Comparatively, the Co $2p_{3/2}$ peak of all five catalysts can be deconvoluted into three major components, primarily Co^{3+} (lower binding energy), Co^{2+} (higher binding energy) and a satellite feature at 790 eV, respectively. The peaks located at 780.8 eV and 795.4 eV feature a doublet Co^{3+} species while peaks located at higher binding energy of around 783.7 eV and 797.4 eV can be ascribed to a spin doublet Co^{2+} species [22,23]. The deconvolution of Co $2p_{1/2}$ peak for E-CO/O_2, however, revealed that the cobalt species are mostly in the +2 oxidized state, recording the highest Co^{2+}/ Total Co ratio of 0.48. It is also important to mention that both Co $2p_{1/2}$ and Co $2p_{3/2}$ regions have shifted to higher binding energies as compared to the corresponding peak positions reported in literatures [24] indicating a stronger electronic interaction between Co and Ni in all five catalysts. The shift in binding energy is caused by the enrichment of A-site cations in which the A/B ratio increases as it fills the A-site vacancies and this possibly contributes towards the confinement of the exsolved particles during exsolution [25]. The Ni 2p spectra (Figure 4 (b)) revealed the presence of only Ni^{2+} with two satellite peaks in all five samples. The fitting peaks of Ni $2p_{3/2}$ and Ni $2p_{1/2}$ at 857.4 eV and 875.1 eV, respectively are both assigned to Ni^{2+}. Two intense satellite peaks of nickel are also observed at 863.5 eV and 881.5 eV [26]. These XPS data indicate that in all five catalysts, nickel exists in the Ni^{2+} state [22].

The O1s XPS spectra, presented in Figure 4 (d) shows that all catalysts comprise of three types of surface oxygen species, including lattice oxygen species ($O_{latt.}$) and chemisorbed oxygen species; namely the oxygen defect ($O_{deff.}$) and adsorbed oxygen ($O_{ads.}$) species. $O_{latt.}$, in particular, depending on its binding energy, it can heavily

affect the selectivity of various conversion of CH_4 and CO_x [27,28]. Although the prepared catalysts have similar formulation, the difference in exsolution agent and pretreatment can alter the binding energy and intensity of the oxygen species present in the catalysts, as a result of various active metals incorporation. When CO was used as the exsolution agent (E-CO and E-CO/O_2) or in the pretreatment (RO2% and RO18%), it promotes the formation of $O_{latt.}$, but at a lower binding energy, advocating a lower CO selectivity during the oxidation process. H_2 as a stronger reducing agent enabled the formation of $O_{latt.}$ at a higher binding energy, signifying a stronger CO selectivity in E-H. RO18% encompassed the benefits of $O_{latt.}$ formation both at higher binding energy and with the addition of RO pretreatment, further promoting the $O_{latt.}$ formation of the catalyst.

The chemisorbed oxygen species ($O_{deff.}$ and $O_{ads.}$) were also considered as the important reactants that enable the oxidation of CO into CO_2 during the oxidation [29,30]. Oxygen defect (Odeff) represents the oxygen anion defect or vacancy that regulate the intrinsic properties of perovskite catalyst such that it enables faster transfer of surface charge and these peaks are located around 530.9 eV for all catalysts [23]. The ratio of chemisorbed and lattice oxygen species, ($O_{ads.}$ + $O_{deff.}$)/$O_{latt.}$ for all catalysts are listed in Table 2 as a way to ascertain the effect of chemisorbed oxygen species towards their catalytic activities. Even though RO2% recorded the highest ($O_{ads.}$ + $O_{deff.}$)/$O_{latt.}$ ratio, but since it has the lowest $O_{latt.}$/ O_{Total} ratio, it did not lead to a good performance in the CO oxidation process. RO18% with moderate ($O_{ads.}$ + $O_{deff.}$)/$O_{latt.}$ ratio recorded the highest $O_{latt.}$/ O_{Total} ratio, is expected to exhibit excellent catalytic performance in comparison with others, especially at higher temperatures with no degradation. This is aligned with the findings earlier where perovskite catalyst with improved $O_{latt.}$ can attract CO for oxidation process with the available surface absorbed $O_{deff.}$ and O_{ads} [31]. After the reaction, the oxygen vacancies will then refill with absorbed surface oxygen species and bulk lattice oxygen species, demonstrating that the presence of $O_{deff.}$ on the catalysts highly influences the ability of perovskite catalysts to replenish their oxygen [32]. E-H, which was exsolved using H_2, has a low amount of $O_{deff.}$, limiting its' catalytic activity since the replenishment of oxygen on the catalyst's surface is lower. When CO was included in the exsolution process (E-CO, E-CO/O_2, RO2% and RO18%), the $O_{deff.}$ showed prominent increase and potential improvement in surface oxygen species replenishment, which is expected for continuous reaction. Combining these with the previous data, a good perovskite catalyst should denote a high amount of $O_{latt.}$ that can attract CO for reaction, high $O_{ads.}$ and $O_{deff.}$ on the surface that are readily available for reaction and high $O_{deff.}$ for faster replenishment of surface oxygen species.

The area under the deconvoluted peaks was used to quantify the proportion of the species on the surface of the catalysts and the results are

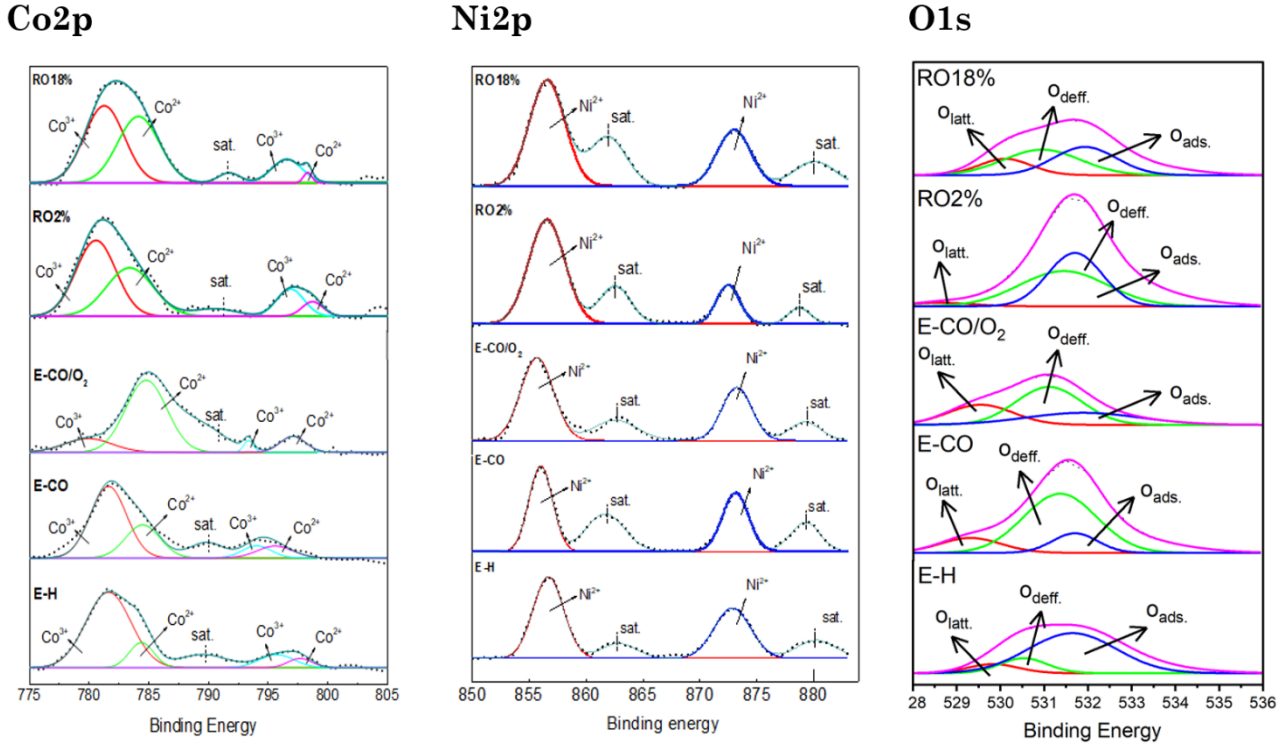

Figure 4. The XPS spectra of (a) Co 2p, (b) Ni 2p and (c) O 1s for E-H, E-CO, E-CO/O2, RO2% and RO18%.

listed in Table 2. The Co/Ni molar ratio is in good agreement with the EDX analysis, confirming the exsolution of Co and Ni in the order of E-CO<RO2%<RO18%<E-CO/O_2<E-H. This result shows that H_2 promotes greater Co exsolution (3.36 times higher exsolution than that of E-CO and 2.46 times higher than that of E-CO/O_2) compared to when CO and CO/O_2 were used as the exsolution agent. The Co/Ni molar ratio of 2.44 and 2.27 were recorded for RO2% and RO18%, respectively, showing an increase in the Ni content, although these contradict those recorded in the EDX results. The computed Co^{2+}/ Co^{3+} molar ratio of E-H, E-CO, RO2% and RO18% are comparatively low (0.21, 0.53, 0.68 and 0.75 respectively), as compared to when the catalyst was subjugated in a redox (E-CO/O_2) exsolution environment, indicating the presence of higher Co^{2+} as opposed to Co^{3+} on the surface of E-CO/O_2. Based on the XPS analysis, both Co^{2+} and Co^{3+} for Co and Ni^{2+} for Ni coexist in all five samples, with E-CO/O_2 comprising of significantly higher amount of the potentially inactive Co^{2+}. Not only that, increasing the CO content to 18% in the redox pretreatment also resulted in lesser Co^{3+}/Co^{2+} ratio, indicating higher amount of Co^{2+} than that of RO2% and E-H.

3.2. CO oxidation activity

The catalytic activity of these catalysts was performed in situ following the exsolution and pretreatment steps. Figure 5 highlights both the CO conversion and CO_2 production rate, $r^*_{CO_2}$ for all five catalysts to distinguish the effectiveness of the exsolution agents and pretreatment in fabricating these catalysts. For E-H and E-CO, the CO conversion and the rate of CO_2 production were initiated at 280 °C, but for E-CO/O_2, the initial reaction started at a slightly lower temperature of 240 °C, demonstrating its capability to operate at lower temperature. The order of the CO oxidation activity can be distinctly tiered as E-H (T_{20}=300 °C), E-CO/O_2 (T_{20}=380 °C) and E-CO (T_{20}=430 °C). Notably, deterioration in the CO oxidation activity was observed for both E-CO and E-H after 500 °C as discussed in our previous study, possibly due to the reduced number of active sites following metal agglomeration [13]. These results agree with most literatures, which often report setbacks associated with degradation of transition metals at high temperatures, limiting the commercialization of these cheaper metals as alternatives to noble metals [33,34]. In contrast, no sign of deterioration was observed for E-CO/O_2, showing an increased CO conversion of 56.99 % at 520 °C. This can be ascribed to having more exsolved Ni, which resulted in stronger interaction between the exsolved metals and the stronger metal/ support interaction considering that Ni has better interaction with TiO_2 oxides [35,36], subsequently

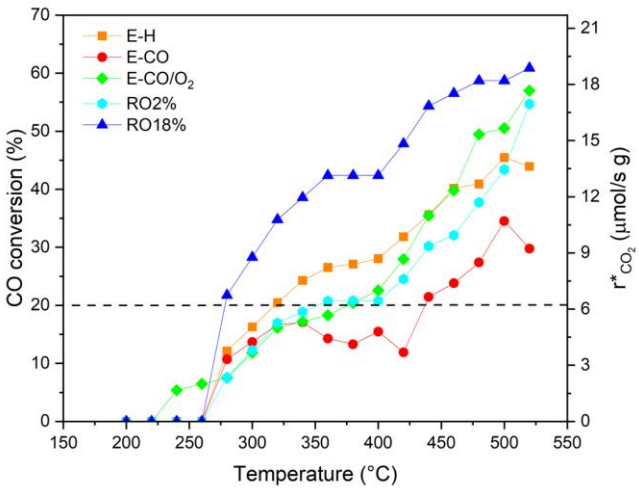

Figure 5. CO conversion and CO_2 production rates, $r^*_{CO_2}$ as a function of temperature for the prepared exsolved CoNi perovskites catalysts. The inlet feed gas comprised a mixture of 2% CO and 1% O_2 balanced with N_2 with a total flowrate, Ft, of 250 mL.min^{-1} and GHSV = 23575.45 h^{-1}. An error below ±10 % was found during the reproducibility test at each measured point.

Table 2. The molar ratio of Co/Ni, Co^{3+}/ Co^{2+} of exsolved CoNi perovskite catalysts prepared with different exsolution agents. Data were obtained from XPS spectra through peak fitting,

Catalyst	Co/Ni	Co^{2+}/ Co_{Total}	$O_{latt.}/O_{Total}$	$O_{deff.}/O_{total}$	$(O_{ads.}+O_{deff.})/O_{latt.}$
E-H	6.92	0.16	0.08	0.12	9.21
E-CO	2.81	0.31	0.11	0.51	5.68
E-CO/O_2	2.35	0.48	0.14	0.27	2.96
RO2%	0.41	0.39	0.02	0.32	27.08
RO18%	0.45	0.41	0.14	0.32	4.36

inhibiting the metals from agglomerating at higher temperatures, preserving the CO_2 production. This also suggests that it is necessary to have moderate amount of Co^{2+} to offset the degradation barrier, demonstrating a slightly different reaction mechanism is at play to fully described the CO oxidation over these catalysts. This contradicts with most literatures where the general consensus is that the octahedrally coordinated Co^{3+} cations primarily serve as active sites for CO oxidation, while tetrahedrally coordinated Co^{2+} are considered to be inactive cations, especially for the spinel structured Co_3O_4 [24,37].

The CO conversions and CO_2 production rates for RO2% and RO18% were also established to ascertain the effectiveness of RO pretreatment on E-H to induce lower Co/Ni ratio and higher Co^{2+} oxidation state as a solution to abate catalyst's degradation. Although the catalyst activity of RO2% and RO18% started at 280 °C, unlike E-CO/O_2, they also achieved the highest CO conversions of 54.72% and 60.87%, respectively at 520 °C with no deterioration. This indicates that with RO pretreatment, a better ratio of Co and Ni were exsolved onto the surface, increasing the interaction between Co, Ni and the perovskites support, reducing the agglomeration at higher temperatures and subsequently inhibiting the occurrence of the deactivation.

The Arrhenius plots (temperature range between 280-520 °C) for all five catalysts are also shown in Figure 6. The corresponding apparent activation energies (E_a) and R^2 values are also summarized in Table 3, considering the first-order reaction in both CO and O_2 for all catalysts. The

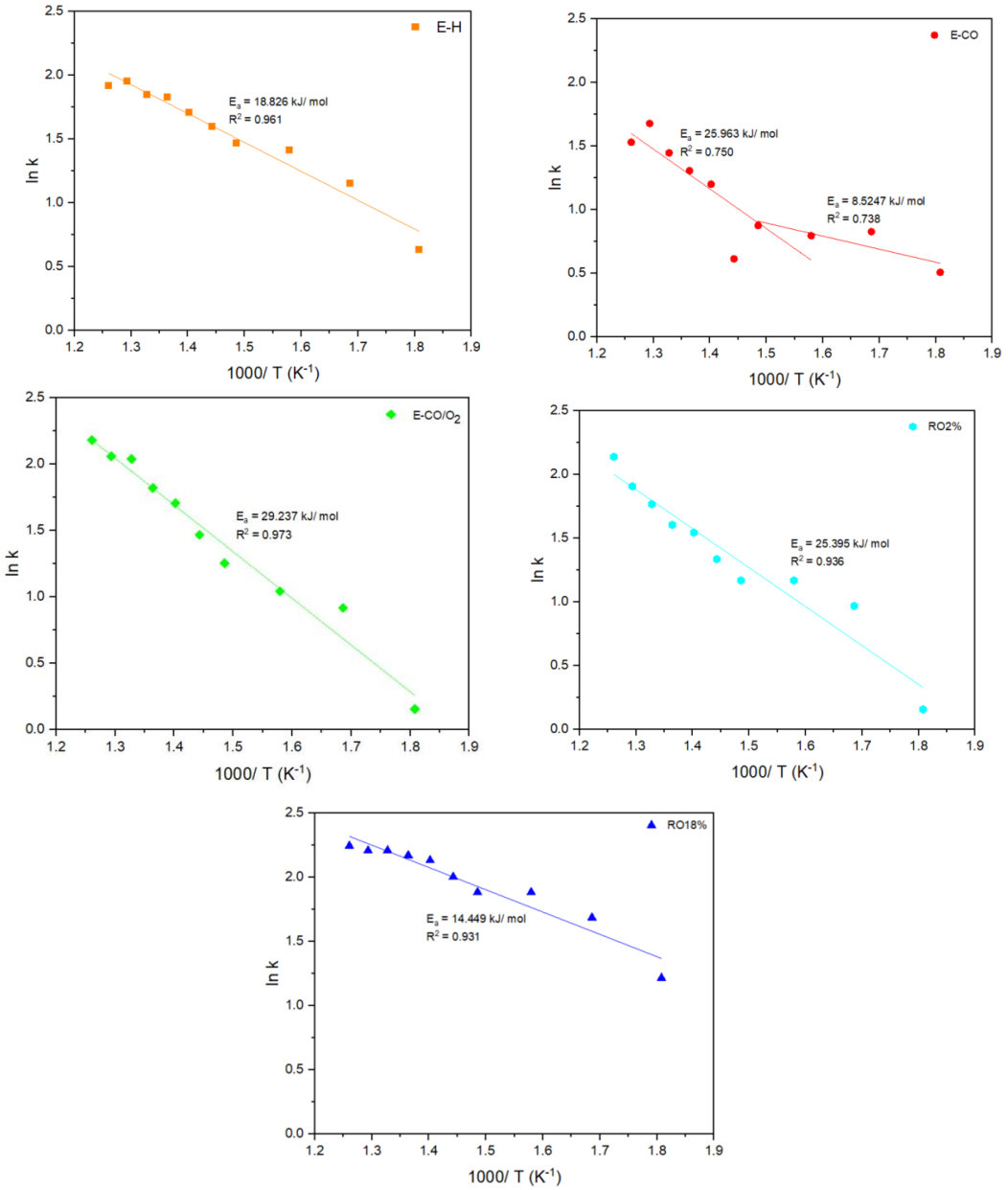

Figure 6. Arrhenius curves for CO conversion as a function of temperature for exsolved CoNi perovskites catalysts.

corresponding activation energies of the catalysts fall within the range observed for similar perovskite materials containing Co and Ni or catalysts for CO oxidation [38,39]. At lower conversion region (280-360 °C), the apparent Ea values follow the same trend as the activity profile with ascending E_a of RO18%<E-H<RO2%<E-CO/O_2 for four catalysts, except for E-CO. E-H recorded Ea of 18.826 kJ/mol which is much lower than that of E-CO/O_2 of 29.237 kJ/mol, indicative of the stronger exsolution power of H_2 compared to CO/O_2. RO18% exhibited the lowest Ea of 14.449 kJ/mol, much lower than the value reported for RO2% (25.395 kJ/mol). These evidences indicated that the existence of O_2 as exsolution agent and lower percentage of CO as the reducing agent in RO pre-treatment may reduce the activity sites and significantly increase the activation barrier of CO conversion in this type of catalyst, which contradicts the results reported by Jiang *et al.* [11]. However, E-CO showed linear variations with the reciprocal of temperatures, but with one inflection point within the temperature range studied. This inflection points of the Arrhenius-type plots can be an indication of a change of the activation energy of the reaction due to the changes in the reaction mechanism with temperature [40]. This might also imply that a different reaction path was induced by the interfacial sites and oxygen of E-CO catalyst [41].

These results suggest that both Co^{3+} and Co^{2+} are the main active sites for these catalysts in CO oxidation, indicating that the CO adsorption and O_2 adsorption/ replenishment steps are crucial. Since the over exsolution of Co onto the perovskite surface are more likely to be oxidized into Co^{3+} during the reaction, the surface Co^{3+} may be inclined to involuntary release O species to react with CO during CO oxidation due to the stronger chemical bonding between Co^{3+} and O^{2-} ions compared to the chemical bonding in compounds with Co^{2+} ions [42], subsequently reducing the catalytic activity of the catalysts. Furthermore, the formation of Co_3O_4 has higher tendency to agglomerate as compared to CoO, reducing the amount of exposed active sites for reaction [43]. Not only that, when redox environment was used to exsolve or pretreated these types of perovskite catalysts, the promoted Ni exsolution may increase the anchorage between the metals with the perovskites, supressing the agglomeration and hindering the formation of Co^{3+} which enables the reaction to continue with the absence of activity degradation at higher temperature. Nevertheless, further study in the future is required to support this observation.

3.3 Proposed Reaction Mechanism

Based on these findings, it has been proposed that the CO oxidation on these catalysts, excluding E-CO follows the Mars–van Krevelen (MvK) mechanism (Figure 7), whereby the reaction mechanism involved the lattice oxygen or adsorbed molecular O_2 on the catalysts' surface (Eqs. 5-8). The gas-phase CO is first adsorbed on a cobalt site (Co^{3+}) and the adsorbed CO reacts with an adsorbed surface oxygen to form gas-phase CO_2 and an oxygen vacancy. The oxygen vacancy formed an excess of 2 electrons, converting the Co^{3+} to Co^{2+}. This is then followed by the O_2 adsorption onto the catalyst surface to replenish the oxygen vacancy. A higher amount of

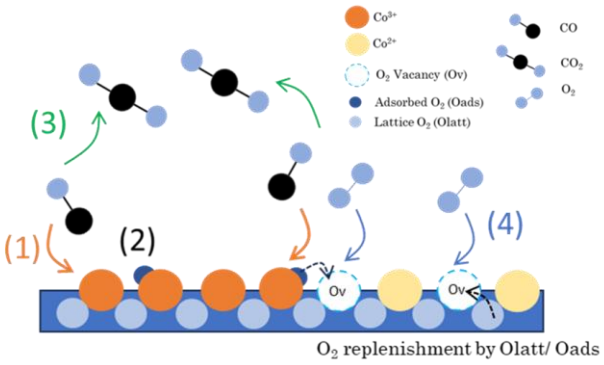

Figure 7. Schematic representation of the proposed MvK mechanism governing the catalytic CO oxidation reaction over E-H, E-CO/O_2, RO2% and RO18%.

Table 3. Activation energies (E_a) and R^2 values for the CO oxidation reaction over exsolved CoNi perovskites catalysts.

Catalyst	Temperature range (°C)	E_a (kJ.mol^{-1})	R^2
E-H	280-520	18.826	0.961
E-CO	280-400	25.963	0.750
	360-520	8.5247	0.738
E-CO/O_2	280-520	29.237	0.973
RO2%	280-520	25.395	0.936
RO18%	280-520	14.449	0.931

lattice oxygen in the perovskites lattice, especially in RO18% can significantly improve the stability of Co^{2+} by enhancing the reduction ability of Co^{2+}, making it easier to convert to Co^{3+}.

$$CO\ (g) \rightarrow CO\ (ads) \quad (5)$$
$$CO\ (ads) + O^{-}\ (ads) \rightarrow CO_2\ (ads) + Ov \quad (6)$$
$$CO_2\ (ads) \rightarrow CO_2\ (g) \quad (7)$$
$$O_2\ (g) + 2Ov \rightarrow 2O\text{-}\ (ads) \quad (8)$$

4. Conclusion

Exsolved A-deficient CoNi perovskites catalysts, $La_{0.7}Ce_{0.1}Co_{0.3}Ni_{0.1}Ti_{0.6}O_3$ with improved CO oxidation activity and without agglomeration at high reaction temperature were successfully fabricated using reduction-oxidation (RO) exsolution agents and RO pretreatment. By introducing CO and CO/O_2 exsolution agents, the exsolution of Ni onto the perovskite surface was improved, strengthening the interaction between exsolved metals and the metal/ support interaction while preventing agglomeration at higher reaction temperatures. The introduction of RO pretreatment further improved the amount of chemisorbed oxygen species (Odeff. and Oads.) while retaining the benefits of standard exsolution process with higher selectivity towards CO. This proves that a good A-site deficient CoNi perovskite catalyst should have a high amount of higher binding energy Olatt. that can attract CO for reaction, high Oads. and Odeff. on the surface that are readily available for reaction and faster replenishment of surface oxygen species. Not only that, over exsolution of active metals that can cause agglomeration should also be eluded since this can hinder the catalytic process. Future research should focus on simulating the CO oxidation over this type of catalysts using density functional theory (DFT) to properly pinpoint the reaction mechanism and support this claim.

Acknowledgements

The authors would like to acknowledge the support from the Fundamental Research Grant Scheme (FRGS) under a grant number of FRGS/1/2018/TK02/UNIMAP/02/8 from the Ministry of Higher Education Malaysia (MOHE). The authors would also like to thank the Centre of Excellence for Frontier Materials Research (CFMR), Universiti Malaysia Perlis (UniMAP), Centre for Research in Advanced Fluid and Processes (UMPSA), Universiti Malaysia Pahang Al-Sultan Abdullah (UMPSA), and Center for Research and Instrumentation Management (i-CRIM), Universiti Kebangsaan Malaysia (UKM) for assisting in sample characterizations throughout this work.

CRediT Author Statement Author

Author Contributions: Lew Guo Liang: Methodology, Investigation, Data Analysis & Curation, Writing - Original Draft. Wan Khairunnisa Wan Ramli: Conceptualization, Methodology, Investigation, Data Validation, Writing - Review & Editing, Supervision, Funding Acquisition. Naimah Ibrahim: Investigation, Writing - Review and Editing. Sureena Abdullah: Investigation, Writing - Review & Editing. All authors have read and agreed to the published version of the manuscript.

References

[1] Takaya, J. (2021). Catalysis using transition metal complexes featuring main group metal and metalloid compounds as supporting ligands. *Chem Sci*, 12(6), 1964–1981. DOI: 10.1039/D0SC04238B.

[2] Reek, J.N.H., de Bruin, B., Pullen, S., Mooibroek, T.J., Kluwer, A.M., Caumes, X. (2022). Transition Metal Catalysis Controlled by Hydrogen Bonding in the Second Coordination Sphere. *Chemical Reviews*, 122(14), 12308–12369. DOI: 10.1021/acs.chemrev.1c00862.

[3] Yu, W., Batchelor-McAuley, C., Chang, X., Young, N.P., Compton, R.G. (2019). Porosity controls the catalytic activity of platinum nanoparticles. *Phys. Chem. Chem. Phys.*, 21(36), 20415–20421. DOI: 10.1039/C9CP03887F.

[4] Zhang, L., Zhu, H., Hao, J., Wang, C., Wen, Y., Li, H., Lu, S., Duan, F., Du, M. (2019). Integrating the cationic engineering and hollow structure engineering into perovskites oxides for efficient and stable electrocatalytic oxygen evolution. *Electrochimica Acta*, 327, 135033. DOI: 10.1016/j.electacta.2019.135033.

[5] Zhu, H., Zhang, P., Dai, S. (2015). Recent Advances of Lanthanum-Based Perovskite Oxides for Catalysis. *ACS Catalysis*, 5(11), 6370–6385. DOI: 10.1021/acscatal.5b01667.

[6] Hwang, J., Rao, R.R., Giordano, L., Katayama, Y., Yu, Y., Shao-Horn, Y. (2017). Perovskites in catalysis and electrocatalysis. *Science*, 358(6364), 751–756. DOI: 10.1126/science.aam7092.

[7] Rojas-Cervantes, M.L., Castillejos, E. (2019). Perovskites as Catalysts in Advanced Oxidation Processes for Wastewater Treatment. *Catalysts*, 9(3). DOI: 10.3390/catal9030230.

[8] Dai, L., Lu, X.-B., Chu, G.-H., He, C.-H., Zhan, W.-C., Zhou, G.-J. (2021). Surface tuning of $LaCoO_3$ perovskite by acid etching to enhance its catalytic performance. *Rare Metals*, 40(3), 555–562. DOI: 10.1007/s12598-019-01360-w.

[9] Pinto, D., Glisenti, A. (2019). Pulsed reactivity on LaCoO3-based perovskites: A comprehensive approach to elucidate the CO oxidation mechanism and the effect of dopants. *Catalysis Science and Technology*, 9(11), 2749 – 2757. DOI: 10.1039/c9cy00210c.

[10] Li, P., Chen, X., Li, Y., Schwank, J.W. (2021). Effect of preparation methods on the catalytic activity of $La_{0.9}Sr_{0.1}CoO_3$ perovskite for CO and C_3H_6 oxidation. *Catalysis Today*, 364, 7–15. DOI: 10.1016/j.cattod.2020.03.012.

[11] Jiang, Y., Zou, L., Zhang, H., Tang, X., Zhou, L., Tian, C., Dai, S. (2024). Revealing pretreatment-induced structure evolution of $LaFeO_3$ supported Au catalyst for CO oxidation reaction. *Nano Today*, 57, 102341. DOI: 10.1016/j.nantod.2024.102341.

[12] Neagu, D., Papaioannou, E.I., Ramli, W.K.W., Miller, D.N., Murdoch, B.J., Ménard, H., Umar, A., Barlow, A.J., Cumpson, P.J., Irvine, J.T.S., Metcalfe, I.S. (2017). Demonstration of chemistry at a point through restructuring and catalytic activation at anchored nanoparticles. *Nature Communications*, 8(1), 1855. DOI: 10.1038/s41467-017-01880-y.

[13] Lew, G.L., Ibrahim, N., Abdullah, S., Wan Daud, W.R., Ramli, W.K.W. (2021). Exsolution enhancement of metal-support CO oxidation perovskite catalyst with parameter modification. In: *IOP Conference Series: Earth and Environmental Science,* DOI: 10.1088/1755-1315/765/1/012078.

[14] Lew, G.L., Ibrahim, N., Abdullah, S., Daud, W.R.W., Ramli, W.K.W. (2021). Exsolution Enhancement of Metal-support CO Oxidation Perovskite Catalyst with Parameter Modification. *IOP Conference Series: Earth and Environmental Science*, 765(1), 12078. DOI: 10.1088/1755-1315/765/1/012078.

[15] Abu Tahari, M.N., Salleh, F., Tengku Saharuddin, T.S., Samsuri, A., Samidin, S., Yarmo, M.A. (2021). Influence of hydrogen and carbon monoxide on reduction behavior of iron oxide at high temperature: Effect on reduction gas concentrations. *International Journal of Hydrogen Energy*, 46(48), 24791–24805. DOI: 10.1016/j.ijhydene.2020.06.250.

[16] Mountapmbeme Kouotou, P., Waqas, M., El Kasmi, A., Atour, Z., Tian, Z.-Y. (2021). Influence of Co addition on Ni-Co mixed oxide catalysts toward the deep oxidation of low-rank unsaturated hydrocarbons. *Applied Catalysis A: General*, 612, 117990. DOI: 10.1016/j.apcata.2021.117990.

[17] Flores-Lasluisa, J.X., Huerta, F., Cazorla-Amorós, D., Morallón, E. (2023). $LaNi_{1-x}Co_xO_3$ perovskites for application in electrochemical reactions involving molecular oxygen. *Energy*, 273, 127256. DOI: 10.1016/j.energy.2023.127256.

[18] Robert, R., Bocher, L., Sipos, B., Döbeli, M., Weidenkaff, A. (2007). Ni-doped cobaltates as potential materials for high temperature solar thermoelectric converters. *Progress in Solid State Chemistry*, 35(2-4 SPEC. ISS.), 447–455. DOI: 10.1016/j.progsolidstchem.2007.01.020.

[19] Luo, Y., Zheng, Y., Feng, X., Lin, D., Qian, Q., Wang, X., Zhang, Y., Chen, Q., Zhang, X. (2020). Controllable P Doping of the $LaCoO_3$ Catalyst for Efficient Propane Oxidation: Optimized Surface Co Distribution and Enhanced Oxygen Vacancies. *ACS Applied Materials and Interfaces*, 12(21), 23789–23799. DOI: 10.1021/acsami.0c01599.

[20] Bo, L., Rim, H.-R., Lee, H.-K., Park, G., Shim, J. (2021). Characterization of NiO and Co_3O_4-Doped $La(CoNi)O_3$ Perovskite Catalysts Synthesized from Excess Ni for Oxygen Reduction and Evolution Reaction in Alkaline Solution. *Transctions of the Korean Hydrogen and New Energy Society*, 32, 41–52. DOI: 10.7316/KHNES.2021.32.1.41.

[21] Aghazadeh, M., Arhami, B., Malek Barmi, A.A., Hosseinifard, M., Gharailou, D., Fathollahi, F. (2014). $La(OH)_3$ and La_2O_3 nanospindles prepared by template-free direct electrodeposition followed by heat-treatment. *Materials Letters*, 115, 68–71. DOI: 10.1016/j.matlet.2013.10.002.

[22] Kosova, N.V, Devyatkina, E.T., Kaichev, V.V (2007). Mixed layered Ni–Mn–Co hydroxides: Crystal structure, electronic state of ions, and thermal decomposition. *Journal of Power Sources*, 174(2), 735–740. DOI: 10.1016/j.jpowsour.2007.06.109.

[23] Yang, Y., Zeng, R., Xiong, Y., DiSalvo, F.J., Abruña, H.D. (2019). Cobalt-Based Nitride-Core Oxide-Shell Oxygen Reduction Electrocatalysts. *Journal of the American Chemical Society*, 141(49), 19241–19245. DOI: 10.1021/jacs.9b10809.

[24] Liu, Z., Li, J., Wang, R. (2020). CeO_2 nanorods supported M–Co bimetallic oxides (M = Fe, Ni, Cu) for catalytic CO and C_3H_8 oxidation. *Journal of Colloid and Interface Science*, 560, 91–102. DOI: 10.1016/j.jcis.2019.10.046.

[25] Khalid, H., Haq, A. ul, Alessi, B., Wu, J., Savaniu, C.D., Kousi, K., Metcalfe, I.S., Parker, S.C., Irvine, J.T.S., Maguire, P., Papaioannou, E.I., Mariotti, D. (2022). Rapid Plasma Exsolution from an A-site Deficient Perovskite Oxide at Room Temperature. *Advanced Energy Materials*, 12(45). DOI: 10.1002/aenm.202201131.

[26] Shi, Y., Li, J., Zhang, B., Lv, S., Wang, T., Liu, X. (2021). Tuning electronic structure of CoNi LDHs via surface Fe doping for achieving effective oxygen evolution reaction. *Applied Surface Science*, 565, 150506. DOI: 10.1016/j.apsusc.2021.150506.

[27] Yu, X., Tao, X., Gao, Y., Ding, L., Wang, Y., Yu, G., Wang, F. (2022). Oxygen Vacancy-Mediated Selective H_2S Oxidation over Co-Doped $LaFe_xCo_{1-x}O_3$ Perovskite. *Catalysts*, 12(2). DOI: 10.3390/catal12020236.

[28] Sim, Y., Kwon, D., An, S., Ha, J.-M., Oh, T.-S., Jung, J.C. (2020). Catalytic behavior of ABO_3 perovskites in the oxidative coupling of methane. *Molecular Catalysis*, 489, 110925. DOI: 10.1016/j.mcat.2020.110925.

[29] Kim, I., Lee, G., Na, H. Bin, Ha, J.-M., Jung, J.C. (2017). Selective oxygen species for the oxidative coupling of methane. *Molecular Catalysis*, 435, 13–23. DOI: 10.1016/j.mcat.2017.03.012.

[30] Boningari, T., Ettireddy, P.R., Somogyvari, A., Liu, Y., Vorontsov, A., McDonald, C.A., Smirniotis, P.G. (2015). Influence of elevated surface texture hydrated titania on Ce-doped Mn/TiO_2 catalysts for the low-temperature SCR of NO_x under oxygen-rich conditions. *Journal of Catalysis*, 325, 145–155. DOI: 10.1016/j.jcat.2015.03.002.

[31] Han, L., Cai, S., Gao, M., Hasegawa, J., Wang, P., Zhang, J., Shi, L., Zhang, D. (2019). Selective Catalytic Reduction of NO_x with NH_3 by Using Novel Catalysts: State of the Art and Future Prospects. *Chemical Reviews*, 119(19), 10916–10976. DOI: 10.1021/acs.chemrev.9b00202.

[32] Yang, J., Hu, S., Fang, Y., Hoang, S., Li, L., Yang, W., Liang, Z., Wu, J., Hu, J., Xiao, W., Pan, C., Luo, Z., Ding, J., Zhang, L., Guo, Y. (2019). Oxygen Vacancy Promoted O_2 Activation over Perovskite Oxide for Low-Temperature CO Oxidation. *ACS Catalysis*, 9(11), 9751–9763. DOI: 10.1021/acscatal.9b02408.

[33] Tang, X., Wang, J., Ma, Y., Li, J., Zhang, X., Liu, B. (2021). Low-temperature and stable CO oxidation of Co_3O_4/TiO_2 monolithic catalysts. *Chinese Chemical Letters*, 32(1), 48–52. DOI: 10.1016/j.cclet.2020.11.008.

[34] Qi, F., Peng, J., Liang, Z., Guo, J., Liu, J., Fang, T., Mao, H. (2024). Strong metal-support interaction (SMSI) in environmental catalysis: Mechanisms, application, regulation strategies, and breakthroughs. *Environmental Science and Ecotechnology*, 22, 100443. DOI: 10.1016/j.ese.2024.100443.

[35] Seemala, B., Cai, C.M., Wyman, C.E., Christopher, P. (2017). Support Induced Control of Surface Composition in $Cu–Ni/TiO_2$ Catalysts Enables High Yield Co-Conversion of HMF and Furfural to Methylated Furans. *ACS Catalysis*, 7(6), 4070–4082. DOI: 10.1021/acscatal.7b01095.

[36] Zhang, L., Wang, F., Zhu, J., Han, B., Fan, W., Zhao, L., Cai, W., Li, Z., Xu, L., Yu, H., Shi, W. (2019). CO_2 reforming with methane reaction over $Ni@SiO_2$ catalysts coupled by size effect and metal-support interaction. *Fuel*, 256, 115954. DOI: 10.1016/j.fuel.2019.115954.

[37] Zhou, M., Cai, L., Bajdich, M., García-Melchor, M., Li, H., He, J., Wilcox, J., Wu, W., Vojvodic, A., Zheng, X. (2015). Enhancing Catalytic CO Oxidation over Co_3O_4 Nanowires by Substituting Co^{2+} with Cu^{2+}. *ACS Catalysis*, 5(8), 4485–4491. DOI: 10.1021/acscatal.5b00488.

[38] Chen, S., Hao, Y., Chen, R., Su, Z., Chen, T. (2021). Hollow multishelled spherical $PrMnO_3$ perovskite catalyst for efficient catalytic oxidation of CO and toluene. *Journal of Alloys and Compounds*, 861, 158584. DOI: 10.1016/j.jallcom.2020.158584.

[39] Pan, K.L., Young, C.W., Pan, G.T., Chang, M.B. (2020). Catalytic reduction of NO by CO with Cu-based and Mn-based catalysts. *Catalysis Today*, 348, 15–25. DOI: 10.1016/j.cattod.2019.08.038.

[40] Dosa, M., Sartoretti, E., Monteverde, A., Bensaid, S., Popescu, I., Marcu, I.-C., Frontera, P., Malara, A., Macario, A., Piumetti, M. (2024). La-based perovskites for autothermal reforming: In-situ electrical conductivity measurements and catalytic study. *Applied Catalysis O: Open*, 192, 206959. DOI: 10.1016/j.apcato.2024.206959.

[41] Lykaki, M., Stefa, S., Carabineiro, S., Pandis, P., Stathopoulos, V., Konsolakis, M. (2019). Facet-Dependent Reactivity of Fe_2O_3/CeO_2 Nanocomposites: Effect of Ceria Morphology on CO Oxidation. *Catalysts*, 9, 371. DOI: 10.3390/catal9040371.

[42] Singh, V., Major, D.T. (2016). Electronic Structure and Bonding in Co-Based Single and Mixed Valence Oxides: A Quantum Chemical Perspective. *Inorganic Chemistry*, 55(7), 3307–3315. DOI: 10.1021/acs.inorgchem.5b02426.

[43] Miranda-López, M.I., Padilla-Zarate, E.A., Hernández, M.B., Falcón-Franco, L.A., García-Villarreal, S., García-Quiñonez, L. V., Zambrano-Robledo, P., Toxqui-Terán, A., Aguilar-Martínez, J.A. (2020). Comparison between the use of Co_3O_4 or CoO on microstructure and electrical properties in a varistor system based on SnO_2. *Journal of Alloys and Compounds*, 824. DOI: 10.1016/j.jallcom.2020.153952.